Journal of Nuclear Materials 471 (2016) 129–135

Contents lists available at ScienceDirect

Journal of Nuclear Materials

journal homepage: www.elsevier.com/locate/jnucmat

Thermophysical properties of USi to 1673 K

J.T. White*, A.T. Nelson, J.T. Dunwoody, D.D. Byler, K.J. McClellan

Los Alamos National Laboratory, Los Alamos, NM, USA

ARTICLE INFO

Article history:
Received 10 September 2015
Received in revised form
11 January 2016
Accepted 13 January 2016
Available online 18 January 2016

Keywords:
Uranium silicide
USi
Laser flash analysis
Thermal conductivity
Accident tolerant fuels

ABSTRACT

Consideration of uranium silicide compounds as candidate nuclear reactor fuels requires the accurate knowledge of their thermophysical properties as a function of temperature. Stoichiometric USi has received little attention in the literature with regard to property characterization. This absence of data prevents modeling and simulation communities from predicting performance of uranium silicide fuels that are either nominally USi itself, or are designed with other uranium silicide phases but may include appreciable fractions of USi introduced as a result of the fuel synthesis or fabrication process. This study was undertaken to quantify the thermal expansion coefficient, specific heat capacity, thermal diffusivity, and thermal conductivity of USi from ambient conditions to just below the peritectic decomposition of the compound. Stoichiometric samples that were prepared by arc melting and powder metallurgical routes for thermophysical property measurements exhibited 94% USi phase, with the balance being U_3Si_5 phase that likely formed during the solidification process. An energetic phase transformation was observed at 723 K, which is attributed to the inclusion of the secondary U_3Si_5 phase.

1. Introduction

Historic interest in the use of uranium silicides as nuclear fuels has been limited to uranium-rich compounds, such as U_3Si and U_3Si_2, primarily to support the Reduced Enrichment for Research and Test Reactors campaign where heavy metal density is a primary criterion. In recent years, research on uranium-silicon binary compounds has expanded due to their perceived use as an accident tolerant fuel form. Two candidates were initially identified within the uranium-silicon binary system: U_3Si_2 is proposed due to its the higher uranium-content and superior thermal conductivity, while U_3Si_5 is considered an alternative due to its superior melt point among U–Si compounds and improved high temperature oxidation resistance compared to U_3Si and U_3Si_2 [1].

Both U_3Si_2 and U_3Si_5 exist as line compounds. Synthesis of either will therefore likely result in USi inclusions within the microstructure. Recent experimental works focused on characterization of U_3Si_2 synthesized via arc melting and powder metallurgy have produced material containing USi ranging from two percent [2] to over ten volume percent [3]. The latter study's levels of USi would be expected to affect both fresh fuel properties as well as in-pile performance. USi has very limited irradiation experience. The available data obtained for relatively low fuel temperatures and very high burnup does not reveal any gross differences in behavior for USi compared to more familiar U–Si compounds such as U_3Si_2 [4]. More extenuative irradiation testing under representative temperatures and burnup conditions is necessary to evaluate the extent that USi inclusions may affect the behavior of nominally U_3Si_2 fuel, but at present it is not possible to evaluate the impact of USi on unirradiated properties of U_3Si_2 or U_3Si_5 given the absence of thermophysical property data for USi.

According to the most recently published phase diagram shown in Fig. 1 [5], a stoichiometric melt of USi initially forms ~6% U_3Si_5 through a peritectic reaction. The solidified USi crystal structure has had some debate in the literature as to whether it is orthorhombic [6] or a complex tetragonal crystal structure with a stoichiometry of $U_{34}Si_{34.5}$[1] [7]. It has been suggested that the orthorhombic phase is an O-stabilized phase with a stoichiometry of U_8 Si_8 O [8]. Physical measurements of USi have largely been overlooked in the literature, the majority being limited to low temperature magnetic and electrical resistivity measurements [9]. Snyder et al. reported the coefficient of thermal expansion on sintered compacts of USi [10], which is one of the only high temperature property measurements found during the literature review.

* Corresponding author.
E-mail address: jtwhite@lanl.gov (J.T. White).

[1] For the purposes of this paper, $U_{34}Si_{34.5}$ will be represented as USi throughout this manuscript.

http://dx.doi.org/10.1016/j.jnucmat.2016.01.013
0022-3115/

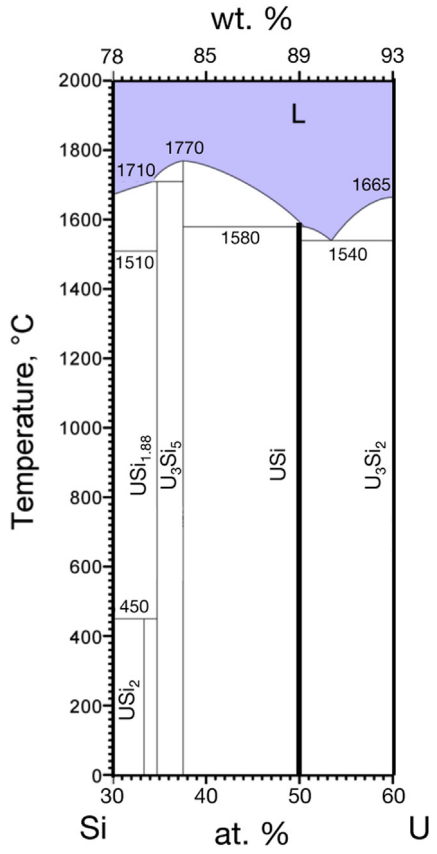

Fig. 1. Truncated uranium-silicon phase diagram adapted from Okamoto [5].

This study was initiated to elucidate the thermophysical properties of USi as a function of temperature to the peritectic decomposition of the material. These experiments will provide properties of USi to enable modeling and simulation communities in validating the use of possible future fuel concepts that intentionally incorporate USi, as well as facilitate assessment of U_3Si_2 or U_3Si_5 processing routes to determine thresholds for permissible USi impurity phase content.

2. Experimental

Specimens for thermophysical measurements of uranium silicide compounds require chemically pure material with minimal oxygen contamination and a methodology to prepare monolithic geometries suitable for the given technique. This study opted to use arc-melting as high purity, homogenous melted material could be synthesized with minimal oxygen contamination. However, excessive cooling rates from the melt induced cracking. As such, a powder metallurgical route was used to fabricate the proper pellet sizes for differential scanning calorimetric (DSC), dilatometry, and laser flash analysis (LFA) measurements. The details regarding sample fabrication and measurement procedures are described in the following sections.

2.1. Sample preparation

Details regarding U–Si sample preparation have been outlined in previous publications [2,11,12]. Minor differences are highlighted between fabrication routes below.

2.2. Sintering USi powder

Chemical purity was determined via inductively coupled plasma optical emission spectroscopy (ICP-OES) on three separate specimens that were prepared from a comminuted button to determine the weight percentage (w/o) of impurity atoms. Approximately 50 mg of the powder was digested in a solution of nitric, hydrofluoric, and hydrochloric acid to perform the ICP-OES analysis, the results of which are shown in Table 1. The majority of the observed impurity elements were consistent with the source material with the exception of Al, which was not included in the certificate of analysis for Si. An Al_2O_3 mortar and pestle was also used to comminute the button specimens prior to analysis. Oxygen and nitrogen concentrations were determined using the inert gas fusion technique (EMGA-920, Horiba, Ltd., Japan). Three samples weighing approximately 100 mg each sampled from an as fabricated button were encapsulated inside tin capsules within an argon glove box prior to measurement. High purity nickel was added as a flux to aid in melting the material.

Specimens for thermophysical property measurements were prepared by a powder metallurgy route. Arc-melted USi buttons were comminuted in a high energy SPEX mill (8000M, SPEX Sample Prep, USA) using a stainless steel jar and milling media and sieved to −200 mesh. All processing was conducted in a N_2(g) glove box, which was maintained below 30 parts per million (ppm) O_2 concentration to minimize oxidation of the powder. Sieved powders were then pressed at 300 MPa in a steel die set utilizing zinc stearate as a die lubricant. Typical green densities ranged from 55% to 65% of the theoretical density. Binders were not used during fabrication of the pellets in order to minimize potential oxygen or carbon contamination. Pellets were sintered using a W metal furnace on W foil under flowing Ar gas using constant heating and cooling rates of 5 K min^{-1} to a maximum temperature of 1773 K for 48 h. Densities were determined using a geometric method. The balance used to determine masses in this study was calibrated to 0.01 mg. Thickness of the pellets were recorded with a digital micrometer to 0.001 mm and the diameter with a digital caliper to 0.01 mm. Resulting pellets were between 96 and 98% of the theoretical density of USi taken as 11.05 g cm^{-3} [13].

2.3. Phase quantification

Specimens for optical microscopy (Axio Imager.M2m, Carl Zeiss AB, Sweden) and scanning electron microscopy (SEM, Inspect, FEI, Hillsboro, Oregon) analyses were conducted on a polished USi sintered pellet that was mounted in epoxy. The sample was initially ground with SiC grinding paper to remove the outer surface, before grinding through 1200 grit SiC. Diamond slurries were applied on decreasing size until a final polish with 0.04 μm colloidal SiO_2 was achieved. It is noted that some degree of pullout was observed following the employed polishing route. A polarized lens was used to distinguish grain size distribution in the material. In order to quantify grain sizes, approximately 500 grains were measured using images similar to the one represented in Fig. 2 (a). The polarized

Table 1
Chemical analysis conducted on as–sintered USi pellets where σ is the standard deviation of the measurement. Elements included in the analysis, but below the detection limit are included as follows: B, Ba, Be, Ca, Cd, Cr, Cu, Fe, Gd, K, Li, Mg, Mo, Mn, Na, Nb, P, Pb, Sb, Se, Sn, Sr, Ta, V, W, Zn, and Zr.

Elements	C	O	N	Al	As	Ni	Co	Ti	Hf
Contents (w/o)	0.08	0.05	0.06	0.54	0.03	0.014	0.009	0.03	0.03
σ (w/o)	0.005	0.03	0.01	0.03	0.005	0.005	0.005	0.005	0.02

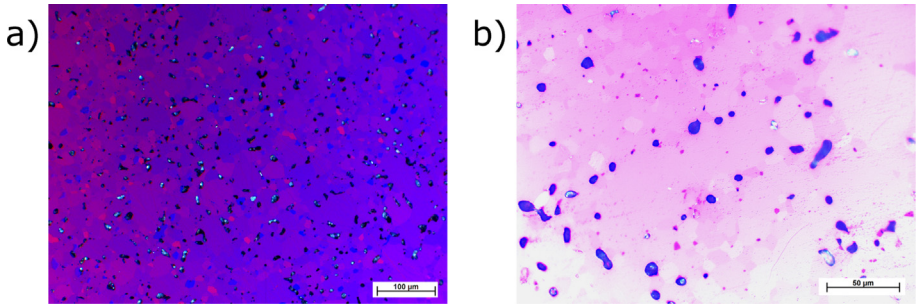

Fig. 2. Microstructure of sintered USi specimen captured in the light microscope using a polarizing light filter (a) to emphasize the grain size of the USi phase, while an oxide precipitate phase is highlighted in (b) after changing the polarization angle.

lens was also utilized to distinguish and quantify the amount of dispersed oxide phase in the matrix, as the oxide did not change with the angle of the polarizing lens, an example of which is shown in Fig. 2 (b). Digital image analysis [14] of the polarized image allowed quantification of the secondary oxide area phase fraction using ~400 particles.

Phase analysis of the fabricated buttons was achieved using a X-ray diffractometer (XRD, D2 Phaser, Bruker Corp., USA). XRD powder specimens were prepared by comminuting an as fabricated button in a mortar and pestle within the glove box. The powder was mounted to a low background Si crystal using a thin layer of vacuum grease before sealing in a polymer dome within the glove box to minimize contact with O_2(g) when the sample was removed from the glove box for analysis. An air scatter lead shield was installed in the polymer dome to minimize the low angle background noise. The XRD used a Bragg-Brentano geometry where the 2θ angle was varied from 10°-60° using a step size of 0.01°.

2.4. Differential scanning calorimetry

Specimens for heat capacity measurements were prepared according to § 2.2 using a 5.2 mm punch and die set. Resulting cylindrical pellets weighed approximately 0.2 g and had diameters of 4.56 mm ± 0.01 mm and had thickness between 1.10 mm and 1.21 mm ± 0.01 mm. Measurements in the DSC used Pt pans with Al_2O_3 liners, which prevented reaction of the USi sample with the pans. Specimen mass varied by Ref. < 0.01 mg between measurements.

The ratio method was utilized to determine the specific heat capacity, c_p, of the specimens in a differential scanning calorimeter (DSC, Pegasus 404C, Netzsch Instruments, Germany). Measurements were conducted at a heating rate of 20 K min^{-1} to a final temperature of 1243 K. Three separate measurements were conducted to indicate the error of the heat capacity measurement, which was determined to be 3% in this study. The atmosphere in the DSC was comprised of ultrahigh purity Ar(g) with 1–10 ppm O_2(g) contamination. Oxygen content on the gas stream was monitored on the exhaust by an in-stream partial pressure of O_2(g), p_{O_2}, sensor (Rapidox 3100 OEM, Cambridge Sensotec, UK), which verified that the atmosphere held during the measurement. Thermocouple calibrations were conducted using melt point standards over the entire range of temperatures investigated. Based on the temperature calibrations, the instrument had an error of ±1 K.

2.5. Dilatometry

The thermal expansion specimen was prepared according to § 2.2 using a 5.2 mm punch and die set. Mass of the thermal expansion specimen was 0.872 g and had diameters of 4.55 mm ± 0.01 mm and thicknesses of 5.09 mm ± 0.02 mm.

Measurement of the linear specimen length change as a function of temperature, dL/L_0, was determined using a dilatometer (DIL 402CD, Netzsch Instruments, Germany). A heating rate of 2.5 K min^{-1} was used to a maximum temperature of 1732 K under an Ar atmosphere. An oxygen sensor was placed on the downstream side of the instrument to monitor oxygen content within the system. Initial p_{O_2} values at the outlet were 1–5 ppm, which dropped to 10^{-12} ppm during the measurement and returned to the initial value on cooling. Specimen mass increased by Ref. <0.5 mg between measurements, which can likely be attributed to surface oxidation of the specimen. A baseline correction was applied to the data to correct for the thermal expansion of the Al_2O_3 fixturing. Using the corrected data, the derivative of the instantaneous length change with respect to temperature was calculated using Proteus 5.2 [15] to provide the physical coefficient of thermal expansion, α_p. Three separate α_p measurements using identical temperature profiles and baseline corrections were used to determine a standard error of 7%.

2.6. Thermal diffusivity measurements

A cylindrical specimen was fabricated according to § 2.2 using a 13 mm punch and die set for LFA measurements with a specimen weight of 2.66 g and a thickness of 2.52 mm ± 0.02 mm. The pellet diameter was typically 11.47 mm ± 0.01 mm in size. Diffusivity values were determined by fitting the temperature rise signal with a modified Cape-Lehman model [16,15]. The error in the recorded sample temperature was determined by measuring the Curie magnetic transition of Fe; the minimum in the diffusivity curve produced was located at 1045.2 K, slightly above the accepted value of 1043 K. As such, an uncertainty of ±3 K is ascribed to the temperatures of each measurement.

The LFA (LFA 427, Netzsch Instruments, Germany) method was utilized to determine the thermal diffusivity, D, of the specimens. In this technique, a laser is pulsed on one side of the specimen, while the heat rise is determined on the opposite side by measuring the infrared blackbody radiation. All surfaces of the sample were coated with a graphite coating (Graphit 33, Kontakt Chemie, Germany) to improve absorption of the laser energy on the bottom face and enhance emissivity of the upper face. Diffusivity data was collected from room temperature to 1673 K in 50 K increments on cooling, collecting three data points per temperature and averaged for the reported value. Typical error derived from the three data points at a given temperature was ≤0.5%. However, repeatability between different samples is conservatively set at 3%. Additional data were collected on heating and were within the experimental error of the technique. The reported data in this study is limited to values taken on cooling. Al_2O_3 fixturing was used throughout the sample

chamber, and gettered argon was again flowed throughout the measurement. Oxygen content of the outlet gas stream was monitored with a p_{O_2} sensor during each measurement and was $<10^{-15}$ ppm for all measurements.

After removal of the graphite coating via immersion in acetone, the sample weighed approximately 1–3 mg greater than the initial mass. This is attributed to a small layer of adsorbed graphite and potential formation of UC at the interface between the USi and carbon coating. Error introduced from thermal expansion of the specimen was calculated from $D = 0.1388 \cdot d^2 \cdot t_{1/2}^{-1}$ [17], where d is the thickness and $t_{1/2}$ is the half-time. Thermal expansion error is calculated at less than 1.5% over the entire temperature range and was not included in this study.

3. Results and discussion

Results for the thermophysical measurements described above are detailed in the following sections. The measured thermal expansion as a function of temperature is used to calculate the temperature–dependent density, $\rho(T)$, relative to the room temperature density value. Thermal conductivity, λ, is calculated as the product of $\rho(T)$, $c_p(T)$, and $D(T)$. The results of all three measurements, along with the calculated λ values are discussed below. The results for each measurement as a function of temperature are compiled in Table A.1.

3.1. Microstructural analysis

A typical microstructure from a sintered and polished USi pellet is shown in Fig. 2 (a), which exhibits a bimodal grain size distribution. The average grain size for the large and small grains is 44 μm ± 14 μm and 8 μm ± 2 μm, respectively. Analysis of the polished pellet with a backscatter detector in a SEM revealed a secondary phase, shown in Fig. 3. Energy dispersive spectroscopic analysis detected enriched Si content relative to the matrix, with no detectable presence of oxygen. Utilization of the aforementioned threshold technique calculated the secondary U–Si phase at 6%. Analysis of the most recently published phase diagram [5] suggests that on cooling, a 93.3% phase fraction of USi balanced with U_3Si_5 should form on cooling from the molten state during the arc melting process. It is believed that the sintered material has retained the phase fractions that resulted from cooling through the liquidus/peritectic temperature. The amount of oxide impurity phase calculated from typical pellet microstructures of Fig. 2 (b) is 0.6% ± 0.4%. The amount of oxide observed from light microscopy is roughly ten times the value measured on the button specimens (Table 1). It is suspected that the powder oxidized while preparing the pellets for sintering, which would present as an oxide impurity phases in the resultant microstructure.

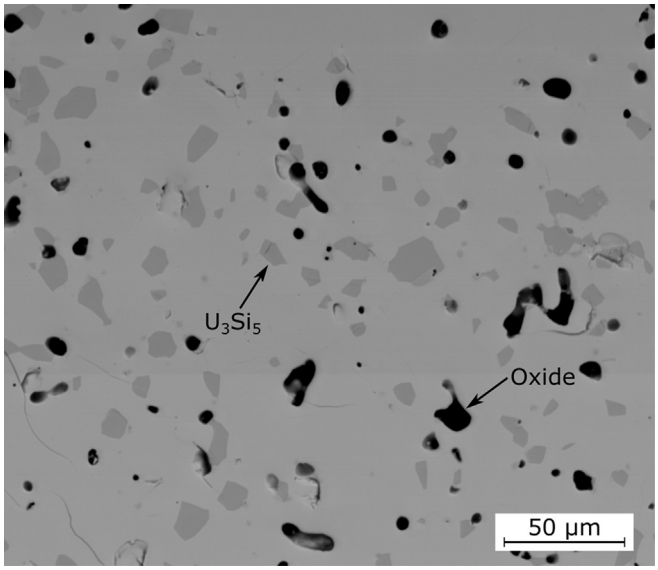

Fig. 3. Representative backscatter SEM microstructure of an as sintered and polished USi specimen. Phases are highlighted based on EDS point analysis of the given phase.

Results for the XRD analysis are shown in Fig. 4. Reference files are included for USi [8] and U_3Si_5 [18]. General agreement is observed with the USi reference pattern, although it is noted many of the reference peaks for U_3Si_5 overlap with USi making deconvolution difficult. The orthorhombic oxygen-stabilized phase is not observed in the XRD analysis of this work, nor peaks representative of UO_2. It is likely that the phase detection limit of the XRD is not sufficient to discern ~ 0.6% phase fraction of oxide material.

3.2. Density and coefficient of thermal expansion

Experimental results for dL/L_0 as a function of temperature to 1673 K are shown in Fig. 5 along with the calculated α_p values (□). Specimen length change from 273 K ≤ T ≤ 353 K are neglected due to the initial nonlinear heating that increases the error in the temperature range. A mean physical coefficient of thermal expansion, $\overline{\alpha}_p$, is calculated at 19.4×10^{-6} K^{-1} with a standard deviation, σ, of 1.4×10^{-6} K^{-1} over entire temperature range. The $\pm\sigma$ is represented by the (----) in Fig. 5. Experimental α_p values are within the standard deviation from 353 K ≤ T ≤ 1450 K. Above 1450 K, experimental α_p values decreased below one σ value relative to the $\overline{\alpha}_p$ and continued to decrease to the maximum temperature determined in this study.

Literature values for the technical coefficient of thermal expansion, α_t, relative to 273 K from sintered compacts measured by Snyder and Duckworth exhibited a linear decrease with increasing temperature for both heating and cooling data [10]. Relative to the $\overline{\alpha}_p$ value calculated above, Snyder's data is within 3%

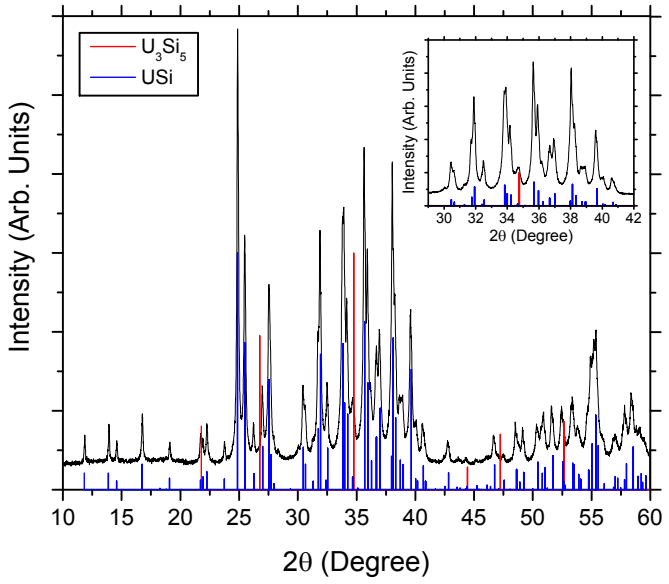

Fig. 4. X-ray diffraction pattern taken from a powder after comminuting an arc-melted button. Powder material was sealed inside of a low background static atmosphere polymer holder. Reference files are included for USi–01-086-0854 [13] and U_3Si_5–04-003-3432 [20]. An inset is included of the intermediate scan region where many of the phases overlap.

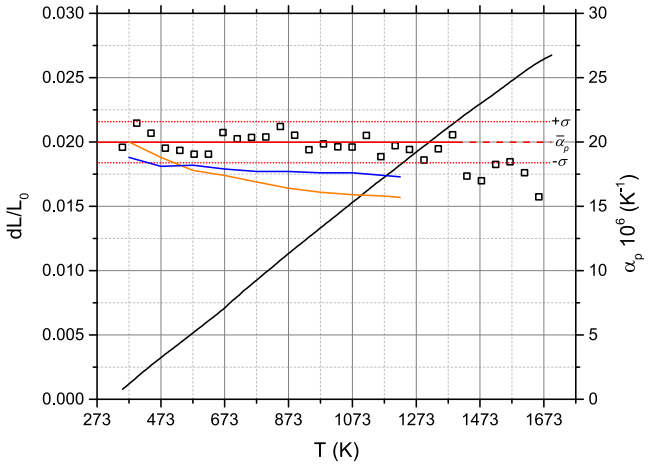

Fig. 5. Thermal expansion of USi as a function of temperature (—) along with α_p (□) measured in this study. The calculated mean physical thermal expansion value, $\bar{\alpha}_p$, is represented by (—) with ± standard deviations, σ (- - -). Snyder's α_T data is included on heating (—) and cooling (—) [10].

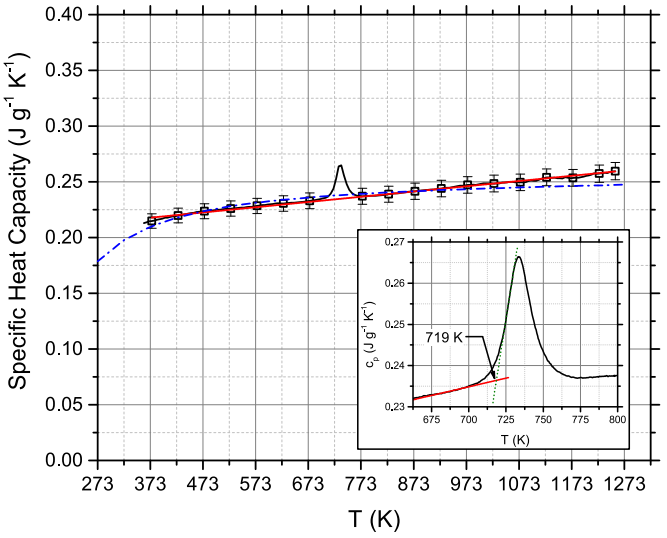

Fig. 6. Specific heat capacity values as a function of temperature for USi as determined by the ratio method. A least squares minimization (—) is included, which disregards the energetic peak at 719 K. Literature values (-·-) are included from Knacke and Oswald [19]. The inset includes the analysis to determine the peak onset temperature.

of the values measured in this study at low temperature and within 10% and 18% at elevated temperatures for the cooling and heating data, respectively. The calculated mean α_p from Snyder's data is 16.6×10^{-6} K^{-1}, which is within 14.5% of the reported value in this study. It is noted that a secondary phase was observed in Snyder's report, but the phase was not identified or quantified. Snyder's samples were prepared by arc-melting followed by sintering of comminuted and compacted powder, similar to the methodology employed in this study. It is suspected that the Snyder's secondary phase is U_3Si_5 and is present in similar quantities to the samples produced in this study. Beyond speculation, it is unclear how the datasets could vary between the this study and Snyder's.

The density as a function of temperature, $\rho(T)$ is calculated in this study using:

$$\rho = \frac{\rho_0}{\left[1 + \bar{\alpha}_p(T - T_0)\right]^3}, \tag{1}$$

where ρ_0 is the reference density determined at room temperature, T_0. The error imparted from the σ in Ref. α_p in calculating ρ is $\leq 0.5\%$ over the entire temperature range investigated in this study.

3.3. Heat capacity of USi

Specific heat capacity of USi as calculated from the ratio method in the DSC as a function of temperature is shown in Fig. 6. An endothermic peak is observed in the DSC signal with an onset temperature of 719 K (see inset of Fig. 6). No physical interpretation of this reaction has been noted in the literature for the USi phase based on the authors' knowledge. A reaction with similar energetics has been observed at 723 K in the U_3Si_5 compound [12], suggestive of a phase transformation in that material. It is suspected that the endothermic peak observed in the DSC signal is a result of U_3Si_5 present at 6% percent by volume. Reference values from the Thermochemical Properties of Inorganic Substances database [19] (-·-) are within 3% of the experimental dataset between 353 K and 1151 K. Above 1151 K, the literature c_p values are within 4.7% of the data determined in this study. A linear regression analysis of the c_p as a function of temperature is represented by (—), which neglected the endothermic peak at 719 K. The results of this analysis are represented by:

$$c_p = 4.59 \times 10^{-5}T + 0.2012\left(\mathrm{J{\cdot}g^{-1}{\cdot}K^{-1}}\right) \tag{2}$$

with a residual sum of squares, $R^2 = 0.994$.

The specific heat capacity in metallic conductors is generally comprised of a phonon, electronic, and dilational components. Calculation of the dilational heat capacity term is complicated in this system as no moduli data was found during the literature review on USi. It is assumed that like most materials that the dilational term is negligible and contributes $\leq$0.1% to the total heat capacity signal over the entire temperature range investigated in this study. Phonon contributions are commonly separated into harmonic and anharmonic terms. The harmonic heat capacity ideally behaves according to the Debye law and asymptotes with the Dulong-Petit value, which is 0.1875 J g^{-1} K^{-1} for USi. Both of the electronic and anharmonic phonon terms are linear with temperature and are commonly expressed as $(b+\gamma)\cdot T$, where b represents the anharmonic term and γ the electronic component. The slope in Equation (2) is the electronic/anharmonic term, which equates to 6.11 mJ mol^{-1} K^{-2} where the data is normalized to a 1-atom basis of $U_{0.5}$ $Si_{0.5}$. Furthermore, the intercept of Equation (2) should equate to the Dulong-Petit value calculated previously. The intercept of Equation (2) is greater than the Dulong-Petit value by 7.3%. The oxide contamination (assumed to be UO_2) or U_3Si_5 secondary phase is insufficient to explain the difference in Dulong-Petit value. It is unclear why this deviation exists.

3.4. Thermal diffusivity and thermal conductivity of USi

Experimental results for the thermal diffusivity determined from LFA measurements as a function of temperature to 1673 K for USi are shown in Fig. 7. The thermal diffusivity data are observed to increase non-linearly with temperature. Additional data collected on cooling from 1273 K is shown in the inset of Fig. 7 near the reaction temperature of 723 K observed in the DSC. A small but measurable discontinuity is observed at ~723 K, where the thermal diffusivity increases by 1.5% compared with the value on heating. A similar increase in thermal diffusivity has been observed in the U_3Si_5 system at the same reaction temperature [12], and it is

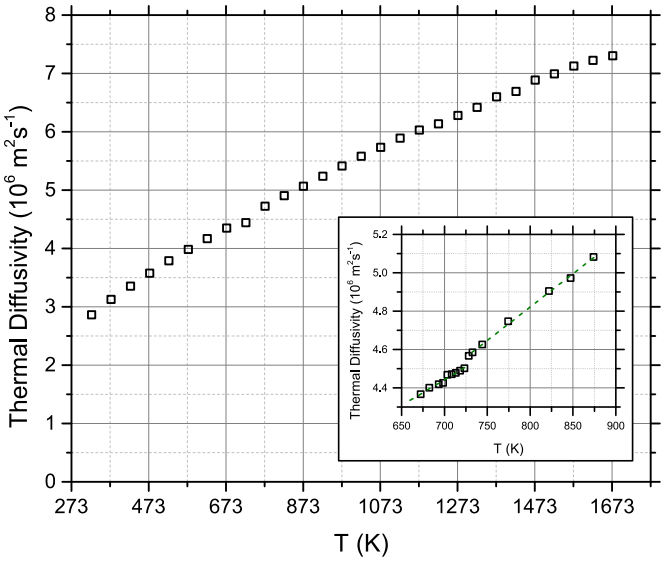

Fig. 7. Thermal Diffusivity data collected on cooling for USi as a function of temperature from 273 K to 1673 K. The inset includes additional data collected near the U_3Si_5 reaction temperature of 723 K.

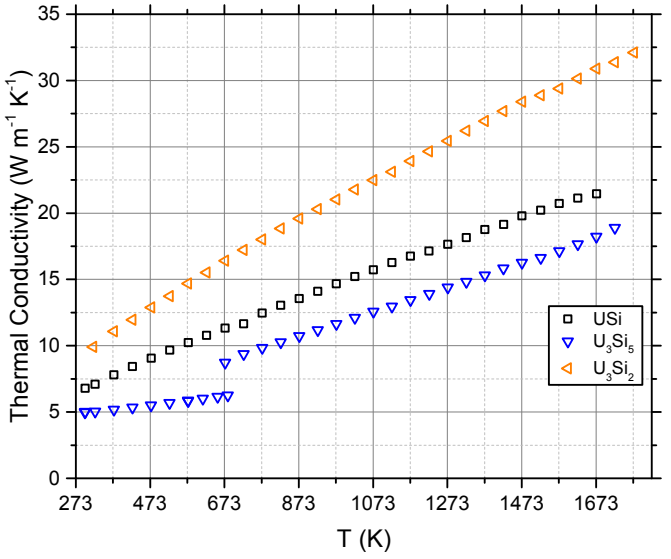

Fig. 8. Calculated thermal conductivity data for USi as a function of temperature to 1673 K collected in this study (□). Literature values for U_3Si_5 (▽– [12]) and U_3Si_2 (◁– [2]) are included for reference.

presumed this is a result of the 6% U_3Si_5 content observed in the microstructure. To the authors' knowledge, no thermal diffusivity exists for the USi phase at the time the literature review was conducted.

Thermal conductivity as a function of temperature as calculated from the $\rho(T)$, $c_p(T)$, and $D(T)$ values determined above is shown in Fig. 8 for USi. Reference values for U_3Si_5 [12] and U_3Si_2 [2] are included for comparison. All of the data has been normalized to 100% theoretical density using:

$$\lambda_{TD} = \frac{\lambda_{exp}}{1 - 3/2(1-P)}, \tag{3}$$

where λ_{TD} and λ_{exp} are the thermal conductivity values for a theoretically dense specimen and experimental values, respectively. The total porosity, P, is calculated from the percent theoretical density value reported in Ref. § 3.1. The influence of secondary phases on thermal conductivity is approximated using the Maxwell equation given the phase volume fraction from microstructural analyses and thermal properties referenced above. An addition of 0.6% UO_2 lowers the effective thermal conductivity of a USi matrix by Ref. ≤0.5%, and is lower than the propagation of error from calculating the thermal conductivity from each of the individual thermophysical properties (5%). Similarly, addition of 6% U_3Si_5 to a USi matrix decreases the effective thermal conductivity by Ref. ≤2.7% over the entire temperature range investigated in this study. Thermal transport in USi increases linearly with temperature according to:

$$\lambda_{TD} = 0.0107 \cdot T + 3.99 \left(\mathrm{W \cdot m^{-1} \cdot K^{-1}}\right) \tag{4}$$

with an R^2 = 0.998. A linear Wiedemann-Franz temperature dependence has been observed for many of the U-rich U–Si compounds, which is indicative of metallic behavior. However, direct comparison is difficult as no resistivity data has been experimentally measured for this compound in the literature.

3.5. Impact of USi impurities on performance of U_3Si_2 or U_3Si_5 nuclear fuels

Assessment of the current results alongside thermophysical property data previously collected for U_3Si_2 and U_3Si_5 by the authors [2,12] reveals that thermal conductivity among the three compounds increases as a function of uranium content at all temperatures investigated (Fig. 8). The presence of USi impurity phases will therefore degrade the thermal conductivity of U_3Si_2 but augment that of U_3Si_5, assuming that the resultant microstructures are nominally continuous (e.g. interphase cracking is minimal). A simple rule-of-mixtures approximation is sufficient to estimate the extent to which the presence of USi would degrade the performance of U_3Si_2. Use of the numerical values reported in this paper and the previous study [2] therefore predict a reduction in thermal conductivity of U_3Si_2 that will scale approximately linearly with USi volume fraction at all temperatures investigated; ten volume percent USi in U_3Si_2 will reduce the thermal conductivity of the fuel to roughly 91% that of pure U_3Si_2.

Determination of heat capacity values resulting from USi inclusions can be similarly determined to first order. Such calculations may be important to assess stored power within a fuel during possible transients. Of more importance may be the difference in thermal expansion between USi and both U_3Si_2 and U_3Si_5. The mean thermal expansion of USi again falls between U_3Si_5 and U_3Si_2. Thermal cycling of U_3Si_2 containing USi may induce interphase cracking given the reduced expansion rate of USi; an analogous concern would arise due to the increased expansion rate of USi when contained in a U_3Si_5 matrix. The rate of temperature change will combine with the materials' mechanical properties to dictate the potential for thermal expansion mismatch to induce cracking in a composite, but the differences in expansion rate of U–Si compounds may represent another criterion that could dictate permissible limits of USi within other U–Si nuclear fuel concepts.

4. Conclusions

The thermophysical properties of USi have been determined as a function of temperature from ambient conditions to 1673 K. A constant value for the coefficient of thermal expansion was

determined as a function of temperature. Specific heat capacity values increased linearly as a function of temperature and are consistent with the data available in the literature. Both the thermal diffusivity and conductivity increase linearly with temperature, which is indicative of metallic conduction.

5. Acknowledgments

The support of the U. S. Department of Energy, Office of Nuclear Energy Fuel Cycle Research and Development program is gratefully acknowledged. This work was performed at Los Alamos National Laboratory which is managed by Los Alamos National Security under contract number DE-AC52-06NA25396. The authors are grateful to A.J. Parkison and A.C Telles in performing the nitrogen and oxygen measurements reported in this study. Additional chemical analyses reported were conducted by ALS Environmental of Tuscon, Arizona (USA).

Appendix A. Tabulated Thermal Property Values Measured in this Study.

Table A.1
Thermophysical property values of USi determined in this study. Values that are *italicized* have been extrapolated from experimental values, as described in the text. Density values have been calculated assuming a constant value of α_p.

T K	$D \times 10^6$ $m^2\ s^{-1}$	c_p $J\ kg^{-1}\ K^{-1}$	$\rho \times 10^{-3}$ $kg\ m^{-3}$	λ $W\ m^{-1}\ K^{-1}$
298	2.75	*215.4*	10.2	6.78
376	3.13	214.8	10.2	7.80
476	3.58	223.7	10.1	9.06
576	3.98	228.4	10.0	10.2
675	4.35	233.0	9.98	11.3
775	4.72	237.1	9.92	12.5
874	5.07	241.5	9.86	13.6
974	5.41	247.3	9.80	14.7
1074	5.73	249.5	9.75	15.7
1174	6.03	253.6	9.69	16.7
1274	6.28	*260.1*	9.63	17.6
1374	6.60	*264.7*	9.57	18.8
1474	6.88	*269.2*	9.52	19.8
1574	7.13	*273.8*	9.46	20.7
1675	7.30	*278.4*	9.41	21.5

References

[1] A. Nelson, J. White, D. Byler, J. Dunwoody, J. Valdez, K. McClellan, Overview of properties and performance of uranium-silicide compounds for light water reactor applications, Trans. Am. Nucl. Soc. 110 (2014) 987–989.
[2] J. White, A. Nelson, J. Dunwoody, D. Byler, D. Safarik, K. McClellan, Thermophysical properties of U_3Si_2 to 1773 k, J. Nucl. Mater. 464 (2015) 275–280.
[3] J.M. Harp, P.A. Lessing, R.E. Hoggan, Uranium silicide pellet fabrication by powder metallurgy for accident tolerant fuel evaluation and irradiation, J. Nucl. Mater. 466 (2015) 728–738.
[4] A. Leenaers, E. Koonen, Y. Parthoens, P. Lemoine, S.V. den Berghe, Post-irradiation examination of AlFeNi cladded U_3Si_2 fuel plates irradiated under severe conditions, Journal of Nuclear Materials 375 (2) (2008) 243–251.
[5] H. Okamoto, Si-U (Silicon-Uranium), in: second ed., in: T.B. Massalski (Ed.), Binary Alloy Phase Diagrams, 3, 1990, pp. 3374–3375. ASM International.
[6] W.H. Zachariasen, Crystal chemical studies of the 5*f*-series of elements. VIII. Crystal structure studies of uranium silicides and of $CeSi_2$, $NpSi_2$, and $PuSi_2$, Acta Crystallogr. 2 (2) (1949) 94–99.
[7] J. Laugier, P. Blum, R. de Tournemine, Sur la veritable structure du compose USi, J. Nucl. Mater. 41 (1) (1971) 106–108.
[8] H. Vaugoyeau, L. Lombard, J. Morlevat, Contribution a l'etude du diagramme d'equilibre uranium silicium, J. Nucl. Mater. 39 (3) (1971) 323–329.
[9] T. Miyadai, H. Mori, T. Oguchi, Y. Tazuke, H. Amitsuka, T. Kuwai, Y. Miyako, Magnetic and electrical properties of the U-Si system (part ii), J. Magnetism Magnetic Mater. 104–107 (1992) 47–48.
[10] M.J. Snyder, W.H. Duckworth, Properties of Some Refractory Uranium Compounds, Technical Report BMI-1223, Battelle Memorial Institute, Sep 1957.
[11] J.T. White, A.T. Nelson, D.D. Byler, J.A. Valdez, K.J. McClellan, Thermophysical properties of U_3Si to 1150 K, J. Nucl. Mater. 452 (1–3) (2014) 304–310.
[12] J.T. White, A.T. Nelson, D.D. Byler, D.J. Safarik, J.T. Dunwoody, K.J. McClellan, Thermophysical properties of U_3Si_5 to 1773 K, J. Nucl. Mater. 456 (2015) 442–448.
[13] T. Le Bihan, H. Noël, P. Rogl, Crystal structure of the uranium monosilicide USi, J. Alloys Compd. 240 (1–2) (1996) 128–133.
[14] C.A. Schneider, W.S. Rasband, K.W. Eliceiri, NIH Image to ImageJ: 25 years of image analysis, Nat. Methods 9 (2012) 671–675.
[15] Proteus Analysis Software, Version 5.2.0, Netzsch-Gerätebau, GmbH, Selb, Germany, 2010.
[16] J. Blumm, J. Opfermann, Improvements of the mathematical modeling of flash measurements, High. Temp. - High. Press. 34 (2002) 515–521.
[17] W.J. Parker, R.J. Jenkins, C.P. Butler, G.L. Abbott, Flash method of determining thermal diffusivity, heat capacity, and thermal conductivity, J. Appl. Phys. 32 (9) (1961) 1679–1684.
[18] K. Remschnig, T. Le Bihan, H. Nöel, P. Rogl, Structural chemistry and magnetic behavior of binary uranium silicides, J. Solid State Chem. 97 (2) (1992) 391–399.
[19] O. Knacke, O. Kubaschewski, K. Hesselmann, Tables, in: Thermochemical Properties of Inorganic Substances, Springer Berlin Heidelberg, 1991, pp. 1–2541.
[20] N. Sato, M. Kagawa, K. Tanaka, N. Takeda, T. Satoh, T. Komatsubara, Magnetic properties of a mass-enhanced ferromagnet U_2 $PtSi_3$, J. Magnetism Magnetic Mater. 108 (1–3) (1992) 115–116.